

Supporting Information for:

Ligand-Free Supermolecules. $[\text{Pd}_2@\text{Ge}_{18}]^{4-}$ and $[\text{Pd}_2@\text{Sn}_{18}]^{4-}$ as Single Bonded Zintl-Ions Cluster Based on $\text{Pd}@\text{Ge}_9$ and $\text{Pd}@\text{Sn}_9$ Assembled Units

Peter L. Rodríguez-Kessler^a and Alvaro Muñoz-Castro^{b*}

^a*Centro de Investigaciones en Óptica A.C., Loma del Bosque 115, Col. Lomas del Campestre, León, Guanajuato, 37150, Mexico.*

^b*Facultad de Ingeniería, Arquitectura y Diseño, Universidad San Sebastián, Bellavista 7, Santiago, 8420524, Chile.*

Content

Figure S1. Isosurface for superatomic shells of *closo*- $[\text{Pd}@\text{Sn}_{12}]^{2-}$ accounting for the 50 cage and 10 4d-Pd electrons, given by $1\text{S}^21\text{P}^61\text{D}^{10}1\text{F}^{14}(4\text{d-Pd})^{10}2\text{S}^22\text{P}^61\text{G}^{10}$ shell structure. **Page 2**

Figure S2. Isosurface for superatomic shells of the $[\text{Pd}@\text{Sn}_9]^{2-}$ unit at the structure given by the overall $[\text{Pd}_2@\text{Sn}_{18}]^{4-}$ cluster. **Page 2**

Figure S3. Isosurface for the bonding or in-phase (+) combinations, and, antibonding or out-of phase combinations (-) between the two $[\text{Pd}@\text{Sn}_9]^{2-}$ motifs within the $[\text{Pd}_2@\text{Sn}_{18}]^{4-}$ oblate cluster. **Page 3**

Table S1. Energy decomposition analysis (EDA) for $\text{Pd}/[\text{Pd}@\text{E}_{18}]^{4-}$ and $\text{Pd}/[@\text{E}_{12}]^{2-}$ interaction, denoting the individual contribution from relevant deformation density channels. **Page 4**

Figure S4. Isosurface for the individual deformation densities ($\Delta\rho_n$) related to the interaction between $[\text{Pd}@\text{Ge}_9]^{2-}/[\text{Pd}@\text{Ge}_9]^{2-}$ (a), $[\text{Pd}@\text{Sn}_9]^{2-}/[\text{Pd}@\text{Sn}_9]^{2-}$ (b), $\text{Pd}/[\text{Pd}@\text{Ge}_{18}]^{4-}$ (c), $\text{Pd}/[\text{Pd}@\text{Sn}_{18}]^{4-}$ (d), $\text{Pd}/[\text{Ge}_{12}]^{2-}$ (e), $\text{Pd}/[\text{Sn}_{12}]^{2-}$ (e). **Page 5**

Figure S5. Contour-plot representation for magnetic response properties under different orientations of the external field (B_z^{ind} , B_x^{ind} , and B_y^{ind}) and their isotropic (averaged) term (NICS), for: $[\text{Pd}@\text{Ge}_{12}]^{2-}$ (a), $[\text{Pd}_2@\text{Ge}_{18}]^{4-}$ (b), $[\text{Pd}@\text{Sn}_{12}]^{2-}$ (c), $[\text{Pd}_2@\text{Sn}_{18}]^{4-}$ (d). **Page 6**

Table S2. Energy decomposition analysis (EDA) at the hybrid TZ2P/PBE0 level of theory for $[\text{Pd}@\text{E}_9]^{2-}/[\text{Pd}@\text{E}_9]^{2-}$ interaction from homolytic fragmentation ($^7[\text{Pd}@\text{E}_9]^{2-}/^7[\text{Pd}@\text{E}_9]^{2-}$), denoting the individual contribution from relevant deformation density channels. **Page 7**

Table S3. Energy decomposition analysis (EDA) at the at the hybrid TZ2P/PBE0 level of theory for $\text{Pd}/[\text{Pd}@\text{E}_{18}]^{4-}$ and $\text{Pd}/[@\text{E}_{12}]^{2-}$ interaction, denoting the individual contribution from relevant deformation density channels. **Page 8**

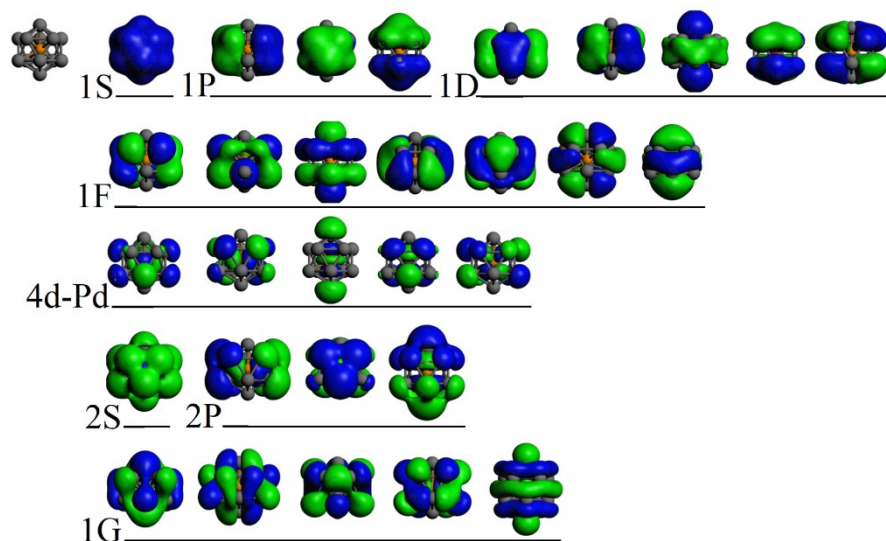


Figure S1. Isosurface for superatomic shells of *closo*-[Pd@Sn₁₂]²⁻ accounting for the 50 cage and 10 4d-Pd electrons, given by 1S²1P⁶1D¹⁰1F¹⁴(4d-Pd)¹⁰2S²2P⁶1G¹⁰ shell structure.

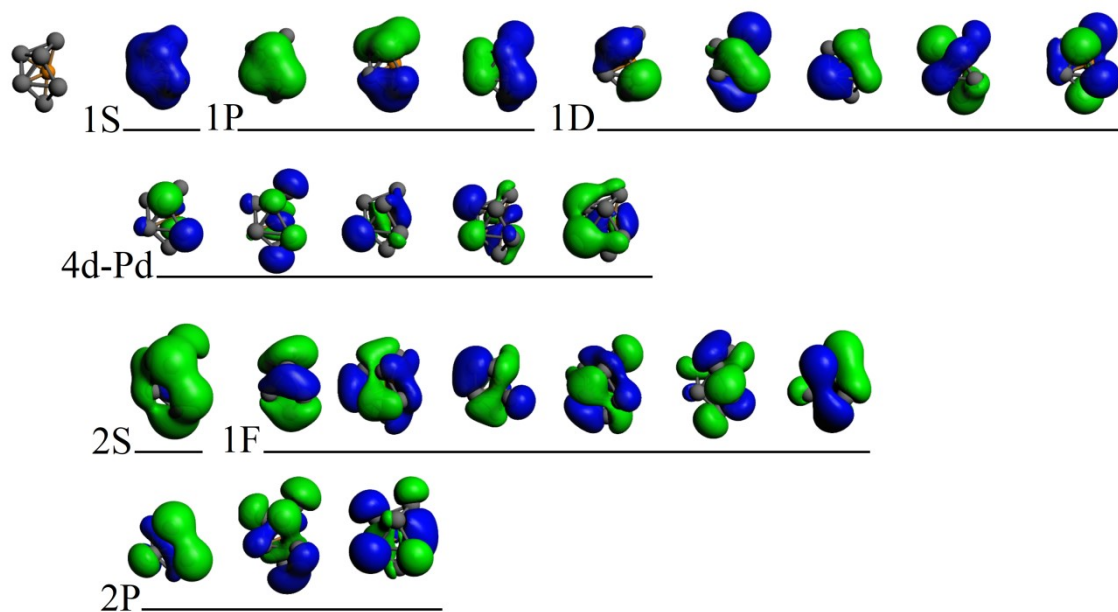


Figure S2. Isosurface for superatomic shells of the [Pd@Sn₉]²⁻ unit at the structure given by the overall [Pd₂@Sn₁₈]⁴⁺ cluster.

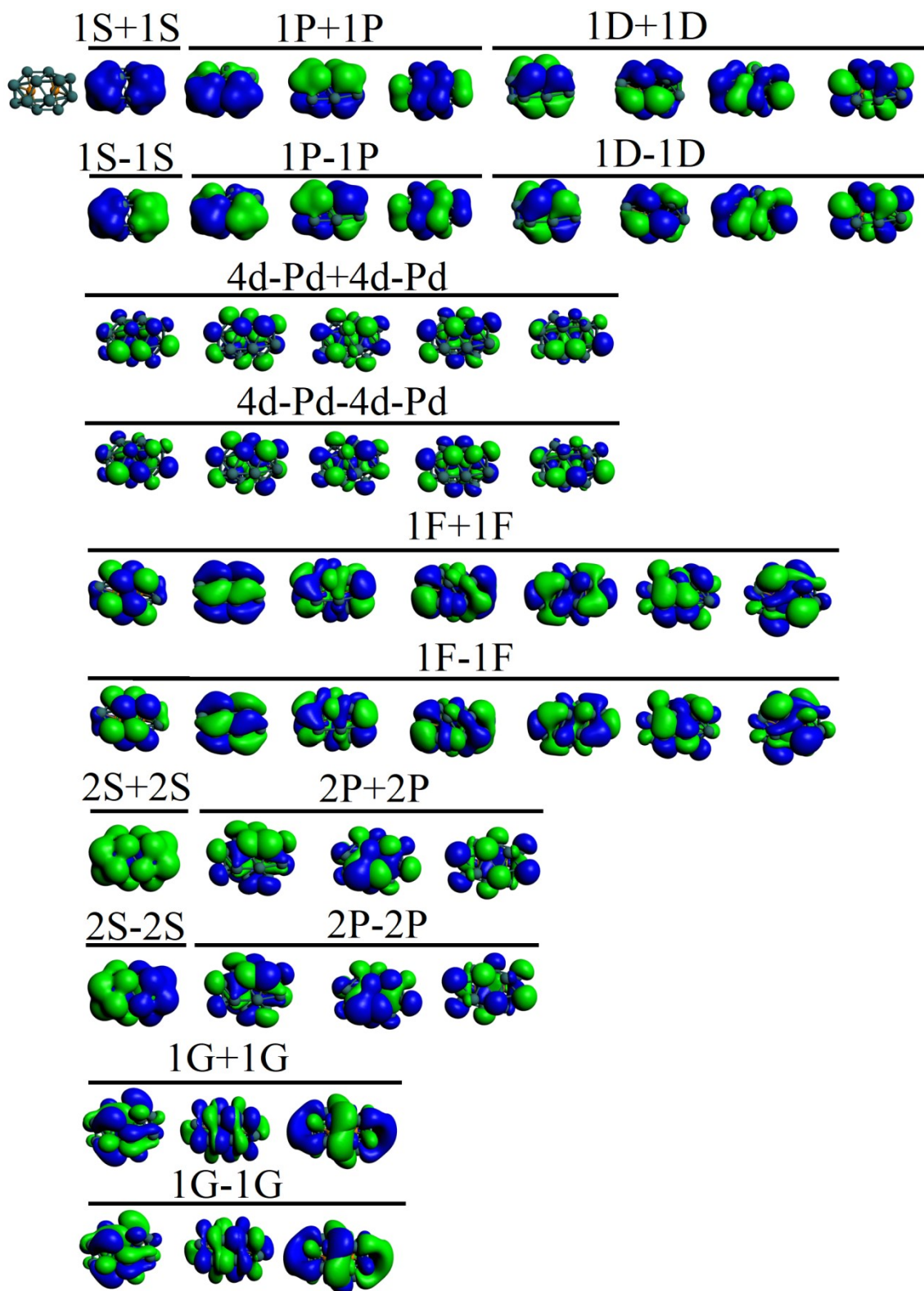


Figure S3. Isosurface for the bonding or in-phase (+) combinations, and, antibonding or out-of phase combinations (-) between the two $[Pd@Sn_9]^{2-}$ motifs within the $[Pd_2@Sn_{18}]^4$ oblate cluster.

Table S1. Energy decomposition analysis (EDA) for Pd/[Pd@E₁₈]⁴⁻ and Pd/[@E₁₂]²⁻ interaction, denoting the individual contribution from relevant deformation density channels. Values in kcal/mol.

	E=Ge		E=Sn	
Pd/[Pd@E ₁₈] ⁴⁻				
ΔE_{Pauli}	334.9		278.3	
$\Delta E_{\text{elestat}}$	-307.6	68.0%	-277.8	70.2%
ΔE_{orb}	-137.8	30.5%	-109.8	27.7%
ΔE_{disp}	-6.8	1.5%	-8.2	2.1%
ΔE_{int}	-117.3		-117.6	
$\Delta \rho_1$	-31.7	23.0%	-23.9	21.8%
$\Delta \rho_2$	-31.7	23.0%	-23.9	21.8%
$\Delta \rho_3$	-23.4	17.0%	-12.0	10.9%
$\Delta \rho_4$	-18.0	13.1%	-14.0	12.8%
$\Delta \rho_5$	-18.0	13.1%	-12.7	11.6%
$\Delta \rho_6$	-7.2	5.2%	-12.7	11.6%
Endo				
Pd/[@E ₁₂] ²⁻				
ΔE_{Pauli}	424.1		303.7	
$\Delta E_{\text{elestat}}$	-369.5	69.5%	-293.1	69.5%
ΔE_{orb}	-157.6	29.7%	-122.7	29.1%
ΔE_{disp}	-4.3	0.8%	-6.1	1.4%
ΔE_{int}	-107.3		-118.1	
$\Delta \rho_1$	-32.6	20.7%	-21.4	17.5%
$\Delta \rho_2$	-29.8	18.9%	-19.6	16.0%
$\Delta \rho_3$	-29.8	18.9%	-19.6	16.0%
$\Delta \rho_4$	-27.5	17.5%	-18.3	14.9%
$\Delta \rho_5$	-27.5	17.5%	-18.3	14.9%
$\Delta \rho_6$	-5.0	3.2%	-15.0	12.2%

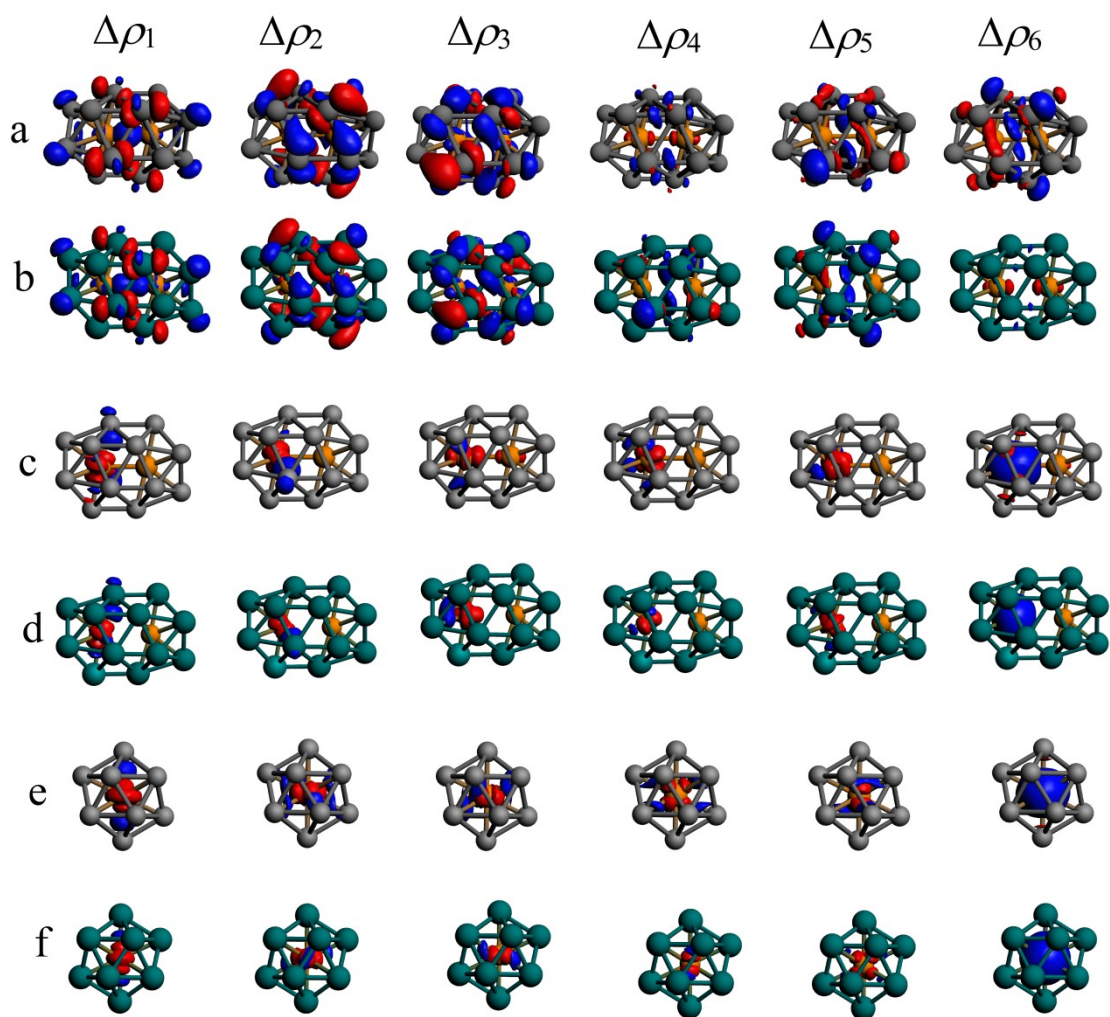


Figure S4. Isosurface for the individual deformation densities ($\Delta\rho_n$) related to the interaction between $[\text{Pd}@Ge_9]^{2-}/[\text{Pd}@Ge_9]^{2-}$ (a), $[\text{Pd}@Sn_9]^{2-}/[\text{Pd}@Sn_9]^{2-}$ (b), $\text{Pd}/[\text{Pd}@Ge_{18}]^{4-}$ (c), $\text{Pd}/[\text{Pd}@Sn_{18}]^{4-}$ (d), $\text{Pd}/[Ge_{12}]^{2-}$ (e), $\text{Pd}/[Sn_{12}]^{2-}$ (e).

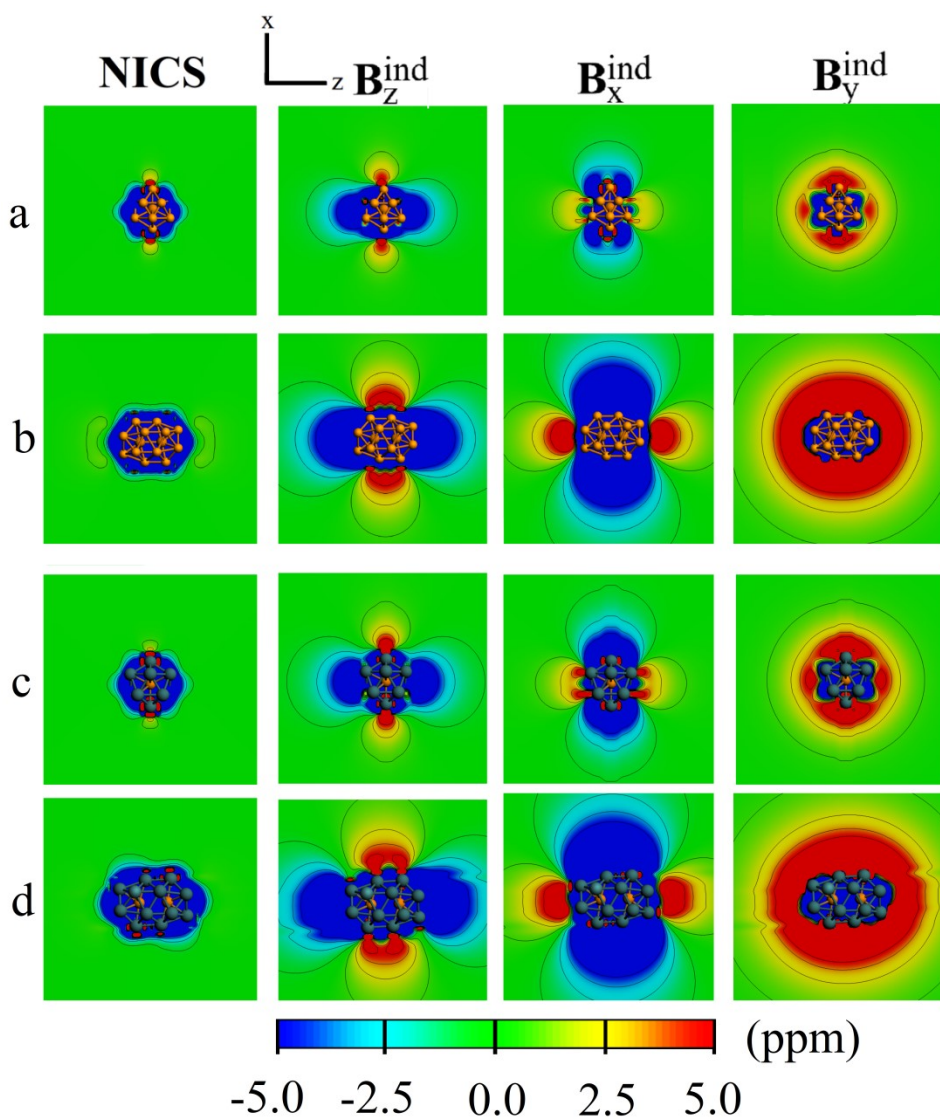


Figure S5. Contour-plot representation for magnetic response properties under different orientations of the external field (B_z^{ind} , B_x^{ind} , and B_y^{ind}) and their isotropic (averaged) term (NICS), for: $[\text{Pd}@\text{Ge}_{12}]^{2-}$ (a), $[\text{Pd}_2@\text{Ge}_{18}]^{4+}$ (b), $[\text{Pd}@\text{Sn}_{12}]^{2-}$ (c), $[\text{Pd}_2@\text{Sn}_{18}]^{4+}$ (d). Color bar between -5.0 to 5.0 ppm, positive values means shielding; negative values means deshielding.

Table S2. Energy decomposition analysis (EDA) at the hybrid TZ2P/PBE0 level of theory for $[\text{Pd}@E_9]^{2-}/[\text{Pd}@E_9]^{2-}$ interaction from homolytic fragmentation ($^5[\text{Pd}@E_9]^{2-}/^5[\text{Pd}@E_9]^{2-}$), denoting the individual contribution from relevant deformation density channels. Values in kcal/mol.

	$[\text{Pd}_2@\text{Ge}_{18}]^{4-}$		$[\text{Pd}_2@\text{Sn}_{18}]^{4-}$	
ΔE_{Pauli}	512.1		481.1	
$\Delta E_{\text{elestat}}$	-176.3	21.3%	-176.1	24.6%
ΔE_{orb}	-629.8	76.2%	-521.0	72.9%
ΔE_{disp}	-20.4	2.5%	-17.7	2.5%
ΔE_{int}	-314.4		-233.7	
$\Delta \rho_1$	-92.0	14.6%	-100.1	19.2%
$\Delta \rho_2$	-92.0	14.6%	-76.8	14.7%
$\Delta \rho_3$	-102.1	16.2%	-76.8	14.7%
$\Delta \rho_4$	-40.7	6.5%	-27.7	5.3%
$\Delta \rho_5$	-34.2	5.4%	-27.7	5.3%
$\Delta \rho_6$	-34.3	5.4%	-26.3	5.1%

Table S3. Energy decomposition analysis (EDA) at the at the hybrid TZ2P/PBE0 level of theory for Pd/[Pd@E₁₈]⁴⁺ and Pd/[@E₁₂]²⁻ interaction, denoting the individual contribution from relevant deformation density channels. Values in kcal/mol.

	E=Ge		E=Sn	
Pd/[Pd@E ₁₈] ⁴⁺				
ΔE_{Pauli}	328.3		257.4	
$\Delta E_{\text{elestat}}$	-307.9	66.6%	-262.7	68.3%
ΔE_{orb}	-147.7	31.9%	-113.9	29.6%
ΔE_{disp}	-6.8	1.5%	-8.2	2.1%
ΔE_{int}	-134.2		-127.4	
$\Delta \rho_1$	-31.7	21.5%	-23.9	21.0%
$\Delta \rho_2$	-31.7	21.5%	-23.9	21.0%
$\Delta \rho_3$	-23.4	15.9%	-12.0	10.5%
$\Delta \rho_4$	-18.0	12.2%	-14.0	12.3%
$\Delta \rho_5$	-18.0	12.2%	-12.7	11.1%
$\Delta \rho_6$	-7.2	4.9%	-12.7	11.1%
Endo				
Pd/[@E ₁₂] ²⁻				
ΔE_{Pauli}	415.7		280.9	
$\Delta E_{\text{elestat}}$	-369.8	68.1%	-277.1	67.5%
ΔE_{orb}	-169.0	31.1%	-127.2	31.0%
ΔE_{disp}	-4.3	0.8%	-6.1	1.5%
ΔE_{int}	-122.8		-128.0	
$\Delta \rho_1$	-32.6	19.3%	-21.4	16.8%
$\Delta \rho_2$	-29.8	17.7%	-19.6	15.4%
$\Delta \rho_3$	-29.8	17.7%	-19.6	15.4%
$\Delta \rho_4$	-27.5	16.3%	-18.3	14.4%
$\Delta \rho_5$	-27.5	16.3%	-18.3	14.4%
$\Delta \rho_6$	-5.0	3.0%	-15.0	11.8%